Supporting Information

Plasmonic Ag-decorated Cu_2O nanowires for boosting photoelectrochemical CO_2 reduction to multi-carbon products

Yanfang Zhang,[a]† Qingmei Wang,[a]† Keke Wang,[a] Yang Liu,[a] Luwei Zou,[b] Yu Zhou,[b] Min Liu,[b] Xiaoqing Qiu,[a] Wenzhang Li, [a,c]* and Jie Li [a]*

[a] School of Chemistry and Chemical Engineering, Central South University, Changsha, 410083, China

[b] School of Physics and Electronics, Central South University, Changsha 410083, China

[c] Hunan Provincial Key Laboratory of Chemical Power Sources, Central South University, Changsha, 410083, China

***Corresponding author e-mails:**

liwenzhang@csu.edu.cn (W. Li), lijieliu@csu.edu.cn (J. Li)

† The authors contributed equally to this work.

Contents

Experiment section

Figures

Figure S1. Schematic illustration for the preparation of Cu_2O/Ag.

Figure S2. Element distribution mapping patterns of Cu_2O/Ag.

Figure S3. XRD patterns of Cu_2O and Cu_2O/Ag.

Figure S4. a) The XPS full survey spectrum and b) O 1s XPS spectra of Cu_2O and Cu_2O/Ag.

Figure S5. a) LSV curves of Cu_2O and Cu_2O/Ag in CO_2 saturated 0.1 M $KHCO_3$ electrolyte. b) LSV curves in CO_2-saturated and Ar-saturated 0.1 M $KHCO_3$ of Cu_2O/Ag.

Figure S6. LSV curves a) and Faradaic Efficiency b) of Cu_2O, Cu_2O/Ag/1, Cu_2O/Ag/3, Cu_2O/Ag, Cu_2O/Ag/10 and Cu_2O/Ag/15.

Figure S7. I-t curves a) and Faradaic Efficiency b) of Cu_2O/Ag under different light intensities (75, 100, 125 mW cm^{-2}).

Figure S8. Mott-Schottky plots measured at different frequencies for a) Cu_2O, and b) Cu_2O/Ag.

Figure S9. CV curves of the photocathodes a) Cu_2O, and b) Cu_2O/Ag; c) the capacitive current densities plotted against scan rates.

Tables

Table S1. Performance comparison with Cu_2O composite photocathode applied in the field of PEC CO_2RR.

Table S2. Electrode interface/electrolyte resistance values (R_{ct}) of Cu_2O and Cu_2O/Ag.

Table S3. Frequency at the minimal value in IMPS plot (f_{min}) and electron transfer time (τ_d) of Cu_2O and Cu_2O/Ag.

1. Experimental section

1.1 Preparation of Cu_2O NWs and Cu_2O/Ag photocathodes

A two-electrode system with a polished copper foil as the working electrode and a platinum sheet as the counter electrode was used for anodic oxidation in 3 M potassium hydroxide solution (3 M KOH) for 8 min to grow $Cu(OH)_2$ NWs at a constant current of 10 $mA \cdot cm^{-2}$. The as-prepared $Cu(OH)_2$ NWs were first calcined at 180 °C for 1 hour to convert to CuO, then annealed at 600 °C for 4 h in an Ar flowing atmosphere to obtain Cu_2O NWs [1]. After the synthesis of Cu_2O NWs, 1 nm, 3nm, 5 nm, 10 nm and 15 nm Ag layers were deposited on the Cu_2O NWs by vacuum thermal evaporation with a growth rate of 0.1 $Å \cdot s^{-1}$. The corresponding samples were named Cu_2O/Ag/1, Cu_2O/Ag/3, Cu_2O/Ag, Cu_2O/Ag/10, and Cu_2O/Ag/15, respectively.

1.2 Morphology and structure characterization

The crystal structures of the samples were recorded by X-ray diffractometer (XRD, D/Max2250, Rigaku) using Cu Kα as radiation source (λ = 0.15406 nm). Scanning electron microscopy (Nova Nano SEM 230, FEI) and high-resolution transmission electron microscopy (HRTEM, Tecnai G2 F20, FEI) were used to record the surface topography of the samples. TU-1901 UV-vis spectrophotometer with integrating sphere was used to record ultraviolet-visible absorption (UV-vis) spectra for analysis of optical properties. X-ray photoelectron spectroscopy (XPS, Thermo Scientific K-Alpha$_+$) with an Al-Kα source was used to determine the elemental composition and valence state of the samples. In situ attenuated total reflection infrared spectroscopy (ATR-IR, Nicolet iS50, Thermo Fisher Scientific) was used to detect

reaction intermediates during CO_2 reduction.

1.3 Photoelectrochemical measurements and CO_2 reduction performance

A series of PEC CO_2 reduction tests were performed using the H-type quartz electrolytic cell. Each cell was filled with 45 mL of 0.1 M $KHCO_3$ electrolyte solution, and the headspace volume of the cell was approximately 55 mL. Before the PEC CO_2RR, CO_2 (99.99%) was purged from the electrolyte in the cathodic compartment for 30 min to 1 h, and then at different potentials (-1.0, -1.1, -1.2, -1.3, -1.4 V vs. Ag/AgCl) for 60 min PEC CO_2RR. The PEC CO_2 reduction products were analyzed by gas chromatograph (GC8860, Agilent, USA) and H NMR spectroscopy (HPLC, Agilent, USA).

PEC measurements were performed at room temperature using an electrochemical workstation (Zahner) under AM 1.5 G illumination (100 $mW \cdot cm^{-2}$). The prepared sample, platinum sheet and Ag/AgCl electrode were used as working electrode, counter electrode and reference electrode, respectively. The electrolyte is CO_2-saturated 0.1 M $KHCO_3$ solution. The H-type quartz electrolytic cell was used and isolated with a Nafion 117 proton exchange membrane. Linear sweep voltammetry (LSV) was performed at a scan rate of 20 mV/s over a potential range of 0.2 V to -1.6 V vs. Ag/AgCl. Mott-Schottky (M-S) plots were acquired under dark at different frequencies (1, 2, 3 kHz) over the potential range of 0.1 to -0.35 V vs. Ag/AgCl. Electrochemical impedance spectroscopy (EIS) was measured from 10 kHz to 100 mHz at -1.0 V vs. Ag/AgCl with an AC amplitude of 10 mV. Intensity-modulated photocurrent spectroscopy (IMPS) was documented by a Zahner CIMPS system at -0.5 V vs.

Ag/AgCl with the frequency range of 100 mHz to 10 kHz. Open-circuit potential (OCP) and transient photocurrent curves were recorded under chopped illumination with 60 s light-on and 30 s light-off. Cyclic voltammetry (CV) curves were measured at different scan rates (10, 20, 30, 40, 50 mV s^{-1}) in the range of -0.2~-0.1 V vs. RHE. The potentials were converted to reversible hydrogen electrodes (RHE) by the following formula:

$$E \text{ (vs. RHE)} = E \text{ (vs. Ag/AgCl)} + 0.059 \times \text{pH} + 0.197 \text{ V} \quad (1)$$

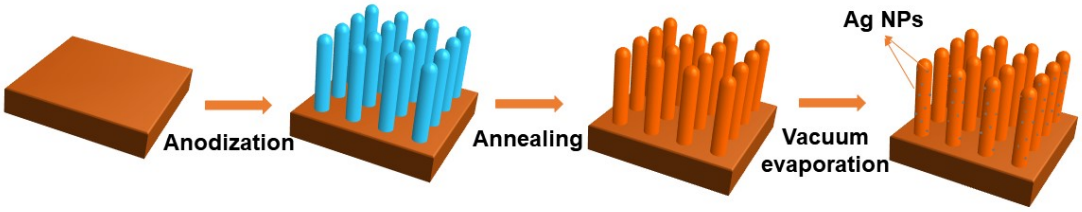

Figure S1. Schematic illustration for the preparation of Cu_2O/Ag.

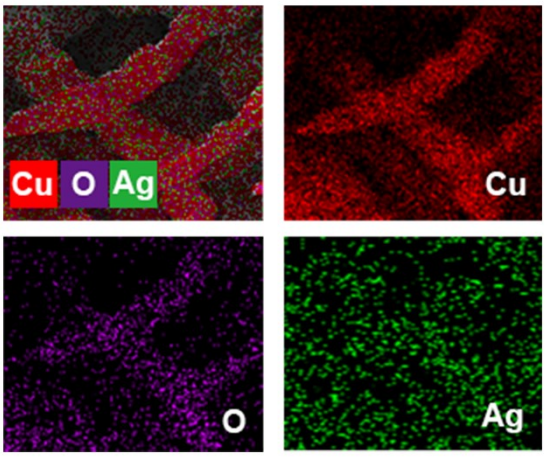

Figure S2. Element distribution mapping patterns of Cu_2O/Ag.

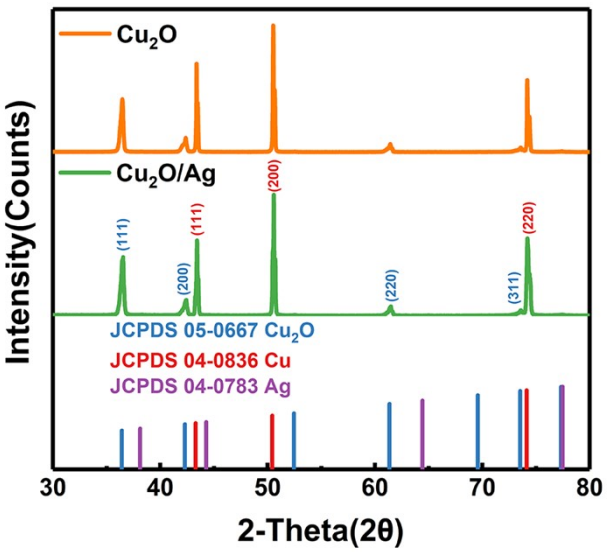

Figure S3. XRD patterns of Cu_2O and Cu_2O/Ag.

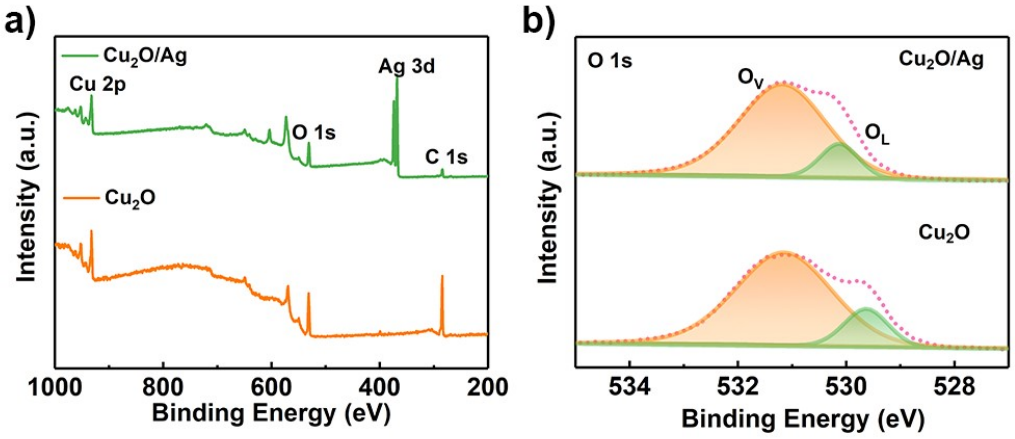

Figure S4. a) The XPS full survey spectrum and b) O 1s XPS spectra of Cu_2O and Cu_2O/Ag.

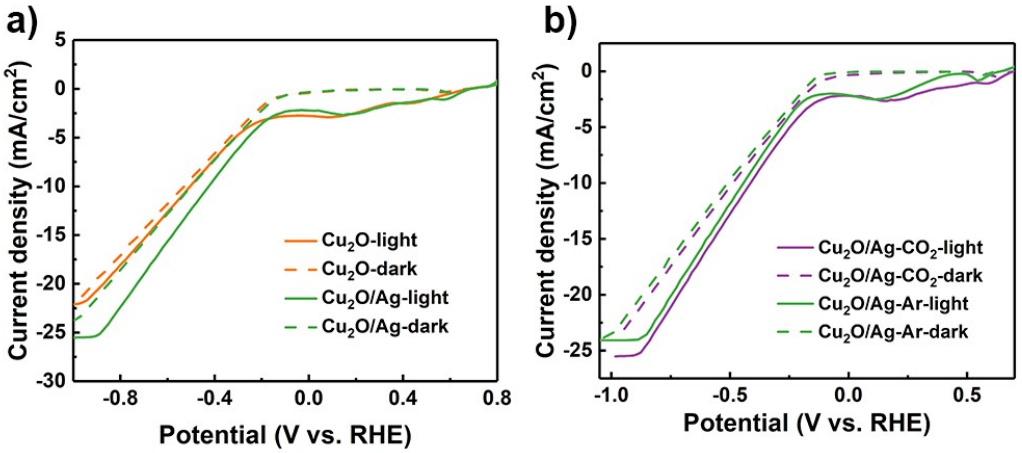

Figure S5. a) LSV curves of Cu_2O and Cu_2O/Ag in CO_2 saturated 0.1 M $KHCO_3$ electrolyte. b) LSV curves in CO_2-saturated and Ar-saturated 0.1 M $KHCO_3$ of Cu_2O/Ag.

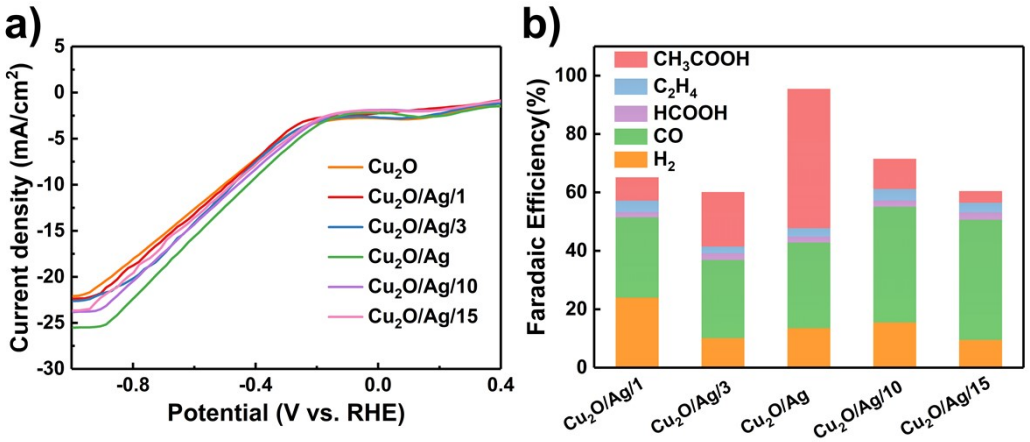

Figure S6. LSV curves a) and Faradaic Efficiency b) of Cu_2O, Cu_2O/Ag/1, Cu_2O/Ag/3, Cu_2O/Ag, Cu_2O/Ag/10 and Cu_2O/Ag/15.

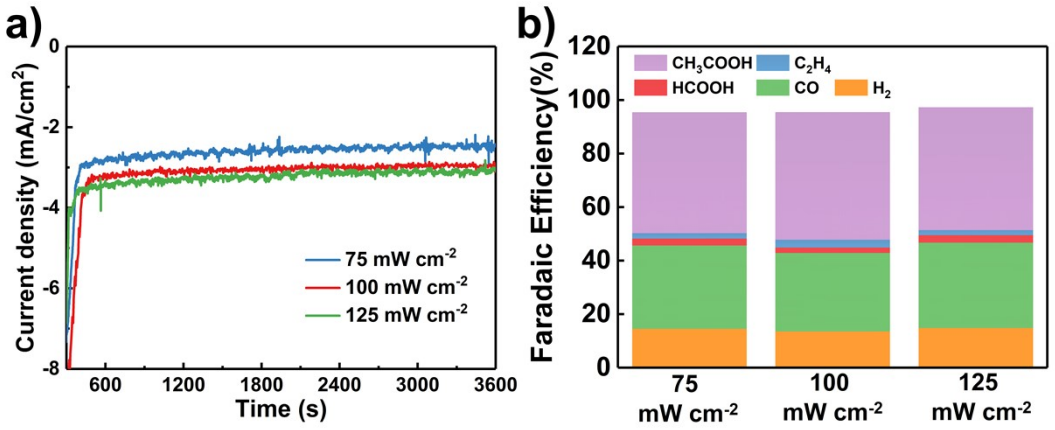

Figure S7. I-t curves a) and Faradaic Efficiency b) of Cu_2O/Ag under different light intensities (75, 100, 125 mW cm^{-2}).

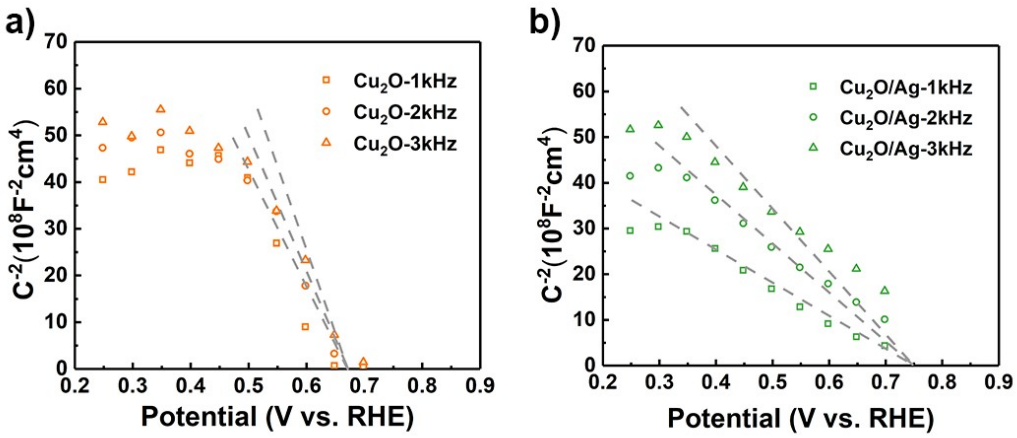

Figure S8. Mott-Schottky plots measured at different frequencies for a) Cu_2O, and b) Cu_2O/Ag.

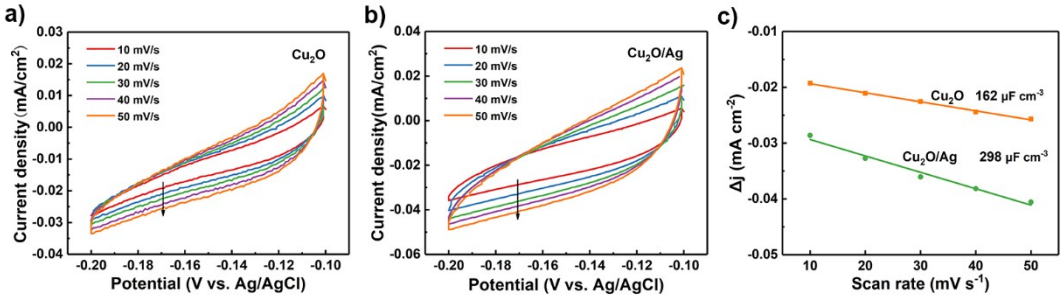

Figure S9. CV curves of the photocathodes a) Cu_2O, and b) Cu_2O/Ag; c) the capacitive current densities plotted against scan rates.

Table S1. Performance comparison with Cu_2O composite photocathode applied in the field of PEC CO_2RR.

Entry	Catalyst	Electrolyte	Potential	Products	FE	Ref.
1	$Cu_3(BTC)_2/Cu_2O$	AcCN/$TBAPF_6$	-1.77 V vs. Fc/Fc^+	CO	95%	[2]
2	Cu_2O/TiO_2/Re(tBu-bipy) $(CO)_3Cl$	AcCN/$TBAPF_6$	-1.73 V vs. Fc/Fc^+	CO	100%	[3]
3	FTO/Fe_2O_3/WO_3/Au/Cu_2O/Ag	AcCN/$TBAPF_6$/TEOA	-1.2 V vs. Fc/Fc^+	C_2H_4	60%	[4]
4	Cu/Cu_2O	0.1 M Na_2CO_3/$NaHCO_3$	0.2 V vs. RHE	CH_3OH	75%	[5]
5	Cu_2O/TiO_2-Cu^+	0.1 M $KHCO_3$	0.3 V vs. RHE	CH_3OH	50.7%	[6]
6	Cu_2O/SnO_x	0.5 M $NaHCO_3$	-0.35 V vs. RHE	CO	74%	[7]
7	Cu_2O/CuO/Pb	0.1 M KOH	-1.6 V vs. RHE	HCOOH, CH_3OH	40.45 %	[8]
8	**Cu_2O/Ag**	**0.1 M $KHCO_3$**	**-0.7 V vs. RHE**	**CH_3COOH**	**47.7%**	**This work**

AcCN: acetonitrile;

$TBAPF_6$: tetrabutylammonium hexafluorophosphate.

Table S2. Electrode interface/electrolyte resistance values (R_{ct}) of Cu_2O and Cu_2O/Ag.

Electrode	R_1/Ω	R_{ct}/Ω
Cu_2O	35.19	15.16
Cu_2O/Ag	34.51	5.11

Table S3. Frequency at the minimal value in IMPS plot (f_{min}) and electron transfer time (τ_d) of Cu_2O and Cu_2O/Ag.

Electrode	f_{min}/Hz	τ_d /ms
Cu_2O	201.03	0.79
Cu_2O/Ag	613.82	0.26

The photogenerated charge transport time (τ_d) of the photocathode can be obtained from IMPS according to the following equation (1):

$$\tau_d = \frac{1}{2\pi f_{min}} \quad (1)$$

where f_{min} represents the frequency at the minimal value in IMPS plot[9].

Reference:

1. J. Luo, L. Steier, M. K. Son, M. Schreier, M. T. Mayer and M. Gratzel, *Nano Lett.*, 2016, **16**, 1848-1857.
2. X. Deng, R. Li, S. Wu, L. Wang, J. Hu, J. Ma, W. Jiang, N. Zhang, X. Zheng, C. Gao, L. Wang, Q. Zhang, J. Zhu and Y. Xiong, *J. Am. Chem. Soc.*, 2019, **141**, 10924-10929.
3. M. Schreier, P. Gao, M. T. Mayer, J. Luo, T. Moehl, M. K. Nazeeruddin, S. D. Tilley and M. Grätzel, *Energy Environ. Sci.*, 2015, **8**, 855-861.
4. G. Liu, F. Zheng, J. Li, G. Zeng, Y. Ye, D. M. Larson, J. Yano, E. J. Crumlin, J. W. Ager, L.-w. Wang and F. M. Toma, *Nat. Energy*, 2021, **6**, 1124-1132.
5. A. A. d. S. Juliana Ferreira de Brito, Alberto José Cavalheiro, and M. V. B. Zanoni, *Int. J. Electrochem. Sci.*, 2014, **9**, 5961-5973.
6. K. Lee, S. Lee, H. Cho, S. Jeong, W. D. Kim, S. Lee and D. C. Lee, *J. Energy Chem.*, 2018, **27**, 264-270.
7. Y. Zhang, D. Pan, Y. Tao, H. Shang, D. Zhang, G. Li and H. Li, *Adv. Funct. Mater.*, 2021, **32**, 2109600.
8. D. H. Won, C. H. Choi, J. Chung and S. I. Woo, *Appl. Catal. B*, 2014, **158-159**, 217-223.
9. Q. Zeng, J. Bai, J. Li, Y. Li, X. Li and B. Zhou, *Nano Energy*, 2014, **9**, 152-160.